Lab on a Chip

RSC Publishing

PAPER

View Article Online
View Journal | View Issue

Cite this: *Lab Chip*, 2013, **13**, 1413

Enhancement of affinity-based biosensors: effect of sensing chamber geometry on sensitivity

N. Scott Lynn Jr., Hana Šípová, Pavel Adam and Jiří Homola*

Received 24th October 2012,
Accepted 31st December 2012

DOI: 10.1039/c2lc41184a

www.rsc.org/loc

Affinity-based biosensing systems have become an important analytical tool for the detection and study of numerous biomolecules. The merging of these sensing technologies with microfluidic flow cells allows for faster detection times, increased sensitivities, and lower required sample volumes. In order to obtain a higher degree of performance from the sensor, it is important to know the effects of the flow cell geometry on the sensor sensitivity. In these sensors, the sensor sensitivity is related to the overall diffusive flux of analyte to the sensing surface; therefore increases in the analyte flux will be manifested as an increase in sensitivity, resulting in a lower limit of detection (LOD). Here we present a study pertaining to the effects of the flow cell height H on the analyte flux J, where for a common biosensor design we predict that the analyte flux will scale as $J \approx H^{-\frac{2}{3}}$. We verify this scaling behavior *via* both numerical simulations as well as an experimental surface plasmon resonance (SPR) biosensor. We show the reduction of the flow cell height can have drastic effects on the sensor performance, where the LOD of our experimental system concerning the detection of ssDNA decreases by a factor of 4 when H is reduced from 47 μm to 7 μm. We utilize these results to discuss the applicability of this scaling behavior with respect to a generalized affinity-based biosensor.

Introduction

Affinity biosensors provide fast and specific means of analyte detection and have become an essential tool for diagnostic and analytic purposes. These devices rely on the capture of a target analyte in liquid media by biomolecules that have been immobilized to an isolated region on the sensor surface. Historically, antigens and antibodies have been the most common biomolecules utilized for sensing purposes;[1] however, there has been a recent surge in the use of several other biomolecules, including DNA or RNA, aptamers,[2] and engineered affinity proteins.[3] Real-time, label-free transduction mechanisms based on optical,[4] mechanical,[5] or electrical[6] methods have the ability to provide data involving not only analyte concentration, but also parameters involved in the kinetics of the affinity relationship. Of these methods, biosensors based on Surface Plasmon Resonance (SPR) have been particularly promising, providing high sensitivities, low limits of detection, and multi-analyte detection.[7]

Along with the steady advancement of sensing transduction technologies, researchers are miniaturizing their sensing platforms and merging them with microfluidic sample delivery methods, providing reductions in required sample volumes as well as increases in sensitivity in a rapid testing format.[8] As the merging of these two technologies become more prevalent, it is increasingly more important (and convenient) to understand how to design and operate each system in order to obtain the highest level of performance. It is therefore desirable to know the geometric and operational parameters that have an influence on the rate of capture (or the rate of reaction) of a target analyte by the immobilized capture probes, or more specifically, the analyte flux (J) to the biomolecules on the sensor surface. An increase in this flux will result in more analyte captured by the sensor over a given time period, which is manifested as an increase in sensor sensitivity and a reduction in the sensor limit of detection (LOD). It should be noted that this study involves the use of sensors that have fluid velocities that are purely axial, where no effort is made to mix the fluid *via* passive or active means. The response of a sensor operated under conditions where the fluid in the sensing chamber is mixed is outside the scope of this study, and we refer the reader to the works by Kirtland and Stroock.[9,10]

The time dependent rate of capture of an analyte by a sensing surface is a function of multiple factors involved in the design and operation of an affinity biosensor. These parameters include the geometry of the microchannel and capture region, the surface density of immobilized capture probes, the molecular diffusivity of the free analyte, the fluid velocity profile in the region surrounding each spot, and the reaction kinetics involved with the affinity interaction. Because many of these parameters may assume values spanning over several orders of magnitude, it is unrealistic to explore the entire

Institute of Photonics and Electronics, Academy of Sciences of the Czech Republic, Chaberská 57, Prague, Czech Republic. E-mail: homola@ufe.cz

parameter space *via* experiment alone. To aid in the survey of this parameter space, researchers often turn to analytical and numerical modeling approaches. There are a variety of analytical solutions that utilize a two-compartment model approach for the calculation of capture rates as a function of the parameters listed above; however, most have difficulties in reliably duplicating rates seen in experimental systems.[11–14] Because of their limited fluid velocities and small characteristic lengths, laminar flow is essentially ubiquitous in microfluidic systems. In this regime, the convection and diffusion of an analyte are well-understood phenomena and can be described by a system of four coupled linear partial differential equations. As a result, there has been a significant rise in the use of computational methods (finite element, finite volume) to simulate the performance of an affinity biosensor without the need of experiment.[15] At this time, however, the computational power to perform a full parameter sweep using these computational methods within reasonable time scales is unavailable.

When possible, analytical solutions can yield insight into how the individual parameters will affect the sensor response. There are several studies providing analytical solutions related to the mass transfer of an analyte to a reactive sensing surface under convective flow (solutions to the classic Lévêque problem); however, each solution is generally limited to a specific operational regime.[16–18] Another simple and powerful tool to yield parameter dependencies is through the use of dimensional analysis.[19] The identification of proper dimensionless quantities from the respective governing equations and boundary conditions can provide an order of magnitude estimate of how the system might scale with each independent parameter. Here we refer the reader to the work by Squires and Manalis, who provide a thorough review of scaling relationships with regard to affinity biosensors.[20]

In this work we aim to enhance the performance of a microfluidic, SPR-based biosensor operating with convective conditions. The sensor has previously been used to detect a variety of analytes, including nucleic acids,[21] proteins,[22] and bacteria cells.[23] Here we examine key design and operational aspects of the sensor in order to increase the sensitivity, and as a result, lower the LOD. The vital components to the sensor, along with the geometry of the microfluidic chamber (flow cell), are shown in Fig. 1. We first derive a scaling solution for the analyte flux to the sensor surface, and identify the microchannel height as a key parameter for sensor performance when the volumetric flow rate through the sensing chamber is held constant. We then verify this predicted scaling behavior towards our affinity-based SPR sensor using both numerical and experimental methods, and discuss the limits of this scaling solution in terms of other affinity biosensing systems. Finally, we highlight this scaling relationship in an experimental system concerning the detection of 20-mer ssDNA using the SPR-based sensor, where we show a reduction in the LOD by over a factor of 4 simply by decreasing the height of the chamber from 47 μm to 7 μm. Despite the vertical placements of the fluidic input and output to the sensing chamber shown in Fig. 1, the results of this study are applicable to a wide range of biosensing platforms utilizing microfluidic methods for sample delivery. Specifically, the results in this study are applicable to rectangular sensing chambers (described by the Cartesian coordinate system), where the active (transducing) surface is confined to a single wall of the chamber.

Theoretical examination

The SPR sensing chamber used in this study is typical of other affinity-based biosensors using microfluidic analyte delivery. A diagram of the sensor used in this study can be seen in Fig. 1. Here we will focus on the sensing chamber itself (Fig. 1B), where the overall design of the sensor shown in Fig. 1A is unimportant for the purposes of this discussion. The sensing chamber consists of SU-8 sidewalls of height H fabricated onto a plastic substrate (CR39), mechanically sealed to a thin gold film on top of a glass slide, where the oval sensing chamber has width W. Two vertical ports (600 μm diameter) drilled through the plastic substrate serve as the fluidic input and

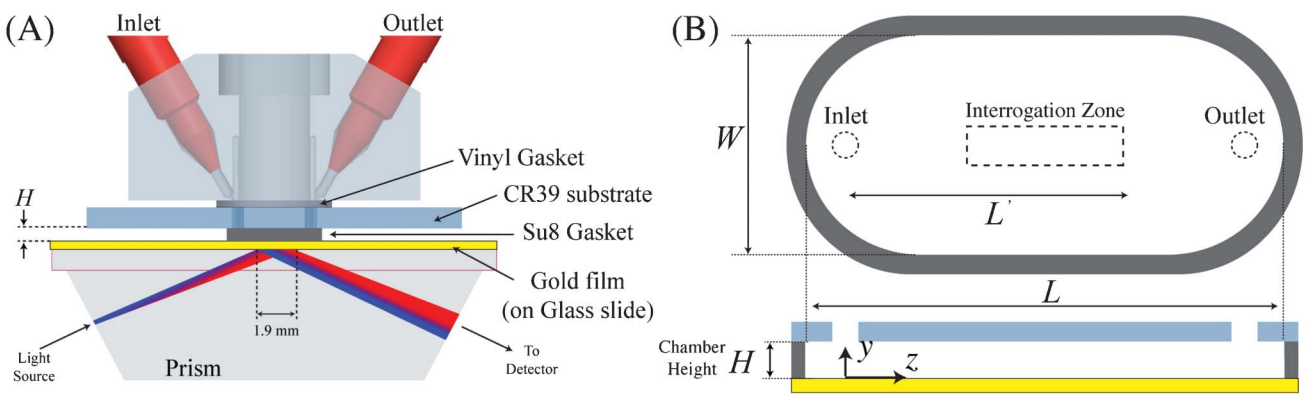

Fig. 1 (A) Detail of the SPR sensor head used in the experimental portion of this study. We utilize an SU-8 gasket to seal the sensing head to the gold surface, which acts as the sensor floor. (B) Geometry of the sensing chamber used in this study.

output. Biomolecule probes are immobilized to the entire floor of the chamber, which acts as the sensor surface and can be characterized as having an overall length L. The parameters relating to the SPR sensor detailed in this study can be seen in Table 1, and are typical of those pertaining to the detection of small ssDNA oligomers.

The response of an affinity biosensor is highly dependent on a number of design (geometrical) and operational parameters, and there are multiple regimes concerning the convection and diffusion of an analyte to the sensor surface.[17,18,20] In order to derive a proper scaling relationship for a sensor of this type, we must know what operational regime it lies in. The two most important parameters in this matter are the channel aspect ratio, $\eta = L/H$, and the mass transfer Péclet number, Pe. For the values of H studied here, the aspect ratio will be in the range of $120 < \eta < 1200$, thus this sensor can be classified under the realm of $\eta \gg 1$.

It should be noted that here we make an important distinction regarding the usual operation concerning these microfluidic sensors. The mass transfer Péclet number relates the relative importance of analyte transport *via* convective means to analyte transport *via* diffusive means. In general, Pe is calculated using the average characteristic fluid velocity U through the sensing chamber, where $U = Q/WH$, and Q is the volumetric flow rate of the analyte solution through the sensing chamber. However, these sensors are typically operated using a constant volumetric flow rate, rather than a constant fluid velocity, regardless of the dimensions of the chamber; therefore, we will define the Péclet number as $Pe = Q/WD$, where D is the diffusivity of the target analyte. The ramifications of this choice will be discussed later in this section.

The sensors utilized in this study will exhibit Péclet numbers of $Pe > 1000$ (seen from the values in Table 1); therefore, the transport of analyte through the sensing chamber in the axial (z) direction will proceed mainly *via* convection. When the analyte solution is introduced into the sensing chamber, molecules close to the sensing surface will have an increased probability of being captured by an immobilized capture probe before being swept out of the sensing chamber. Conversely, molecules further than a distance δ away from the surface will have no interaction with the capture probes and flow through the chamber unperturbed. From this effect we expect an analyte concentration boundary layer with thickness δ to appear over the sensing surface, where $\delta = \delta(z)$ is measured in the y-direction and will increase monotonically with increasing axial distance z.[20] Before we establish an order of magnitude estimate on the relationship between δ and the parameters shown in Table 1, we turn to a model of analyte capture by an immobilized probe. The binding of an aqueous analyte to a capture body can be described using a standard ligand-receptor model,

$$A(aq.) + B(s.) \underset{k_2}{\overset{k_1}{\longleftrightarrow}} AB(s.) \quad (1)$$

where A denotes the aqueous analyte, B the immobilized capture body, AB the immobilized bound complex, and $aq.$ and $s.$ denote the aqueous and solid phases, respectively. Assuming elementary reaction kinetics and ignoring the chance that a captured analyte will diffuse along the surface, the time dependent surface concentration of the bound complex can be described by the relationship

$$\frac{\partial C_{AB}}{\partial t} = k_1 C_{A,s}(C_{B,o} - C_{AB}) - k_2 C_{AB} \quad (2)$$

where k_1 is the association rate constant, k_2 is the dissociation rate constant, and $C_{B,o}$ is the initial (maximum) surface concentration of capture probes, where it follows that $C_{B,o} = C_{AB} + C_B$ with C_B representing the surface concentration of free probes. For the initial stages of the analyte–capture probe interaction ($t \approx 0$), we can estimate the flux of the analyte $J = J(z)$ through the boundary layer to the sensor surface as

$$J = D\frac{\partial C_A}{\partial y} \approx D\frac{(C_{A,o} - C_{A,s})}{\delta} \quad (3)$$

where D is the analyte diffusivity, $C_{A,o}$ is the analyte concentration at the sensor inlet, and $C_{A,s} = C_{A,s}(z)$ is the concentration of analyte just above the sensor surface. In this time period there will be very little bound analyte on the surface, and therefore $C_{AB} \approx 0$. In that case we can estimate the initial reactive flux from eqn (2) as

$$J = k_1 C_{A,s} C_{B,o} \quad (4)$$

By combining eqn (3) and (4) we arrive at a relationship between the bulk and surface concentrations of analyte

$$\frac{C_{A,s}}{C_{A,o}} \approx \frac{1}{1 + k_1 C_{B,o}\delta/D} \quad (5)$$

where the value of $Da = k_1 C_{B,o}\delta/D$ is known as the Damköhler number, which represents the dimensionless ratio of the rate of uptake of an analyte by the immobilized capture probes to the rate of convective and diffusive transport of the analyte to the sensor surface. In the case where $Da \ll 1$, the system falls under the reaction limited regime and $C_{A,s} \rightarrow C_{A,o}$. Here eqn (2) can be solved analytically to obtain the sensor response *vs.* time. This case is rarely applicable to affinity-based biosensors used for analytical purposes, where it is common that $Da \gg 1$ and the system can be classified as mass-transfer limited, with $C_{A,s} \rightarrow 0$.

Table 1 List of parameters utilized in this study

Parameter	Description	Value
L	Length of flow cell	6 mm
H	Height of flow cell	5–50 μm
W	Width of flow cell	2.8 mm
Q	Volumetric flow rate	0.5 $mm^3\ s^{-1}$
D	Analyte diffusivity	$10^{-4}\ mm^2\ s^{-1}$
$C_{B,o}$	Surface density of probes	4×10^{-14} mol mm^{-2}
k_1	Forward reaction coefficient	$10^7\ M^{-1}\ s^{-1}$
k_2	Reverse reaction coefficient	$6 \times 10^{-5}\ s^{-1}$

We now turn our attention to obtain a scaling relationship for the thickness of the analyte concentration boundary layer (δ) to be used in eqn (3) and (5). The sensor detailed in this study has a geometry such that both $L/H \gg 1$ and $W/H \gg 1$, therefore fluid flow in the sensor can be approximated as one-dimensional pressure-driven flow between two flat plates (the results from this assumption will also hold true for geometries such that $H \approx W$). In this case, the axial velocity profile can be calculated as $u_z = u_{\max}(y^2 - H^2/4)$, where $u_{\max} = 3U/2$ is the maximum axial fluid velocity.[24] This parabolic dependence on y creates problems in the derivation of an analytical solution for δ. A general assumption commonly used for this problem is that, for the case where δ is small with respect to H, the fluid velocity u is a linear function of y with a proportionality equal to the fluid shear rate at the microchannel surface, or $u_z \approx \dot{\gamma} y = (\partial u_z/\partial y)y$. For pressure driven flow between two plates, the shear rate at the sensor surface can be calculated as $\dot{\gamma} = 6U/H = 6Q/H^2W$. Given this assumption, we can equate (*i*) the characteristic time τ_c for convection to bring an analyte across the sensor length situated at a height δ above the sensor, $\tau_c \approx L/\dot{\gamma}\delta$, with (*ii*) the characteristic time τ_d for an analyte to diffuse across the boundary layer of thickness δ, $\tau_d \approx \delta^2/D$, providing the relationship

$$\delta \approx L\left(\frac{DH^2W}{6L^2Q}\right)^{\frac{1}{3}} \approx L\left(\frac{1}{6\eta^2 \mathrm{Pe}}\right)^{\frac{1}{3}} \approx L\mathrm{Pe}_s^{-\frac{1}{3}} \quad (6)$$

where $Pe_s = 6\eta^2 Pe$ is the shear rate Péclet number, which relates the overall size of the depletion layer to the length of the sensor. Using the values in Table 1 (along with H = 50 μm) we can calculate a 1st order estimate of Da = 40, and it is safe to assume that this sensor will be mass-transfer limited, where $C_{A,s} \approx 0$ during the initial stages of analyte capture. At this point we assume that during this initial stage, the concentration of bound analyte on the surface is low enough that the reverse reaction (eqn (1)) will essentially be zero, and δ will not be a function of time. Combining eqn (6) and (3) now results in the following expression for J:

$$J \approx \frac{DC_{A,o}}{L}\mathrm{Pe}_s^{\frac{1}{3}} \approx C_{A,o}\left(\frac{6D^2Q}{LH^2W}\right)^{\frac{1}{3}} \quad (7)$$

From eqn (3), it can be seen that for a restricted volumetric flow rate the channel height is the most important geometrical parameter for the sensing chamber. In this regime the flux will scale as $J \approx H^{-\frac{2}{3}}$, and a decrease in H will result in an increase in the sensitivity of the SPR biosensor. Here we see the distinction between experiments that will be conducted with constant U *vs.* those conducted under constant Q, where it follows that the flux will scale as $J \approx H^{-\frac{1}{3}}$ for experiments restricted to constant U. This relationship can provide for significant increases in the sensitivity of a biosensor operating in the regime of both $\eta \gg 1$ and $\mathrm{Pe} \gg 1$. For example, a reduction in H by an order of magnitude from 50 μm to 5 μm should result in an increase in sensitivity by a factor of $(50/5)^{\frac{2}{3}} = 4.6$. In the next sections we utilize both numerical and experimental results to verify these predictions.

Numerical methods

In this study we assume that the rate of interaction between analyte and sensor surface can be modeled with the assumption that the concentration of analyte on the sensing surface is zero (Da $\gg$ 1), and the system exists in a steady state. The validity of this steady-state assumption is examined later in the discussion. We utilize the finite element package COMSOL to solve the Navier–Stokes equations along with the convection–diffusion equation to obtain a solution for the velocity, pressure, and analyte concentration field within the sensing chamber. For each simulation we imposed a boundary condition of $C_{A,s}$ = 0 on the sensor floor, with a constant analyte concentration and a fully developed velocity profile at the chamber inlet (where the inlet was extended 0.5 mm from the top face of the chamber). The simulation mesh was composed of a free triangular scheme in the x,z-plane (variable characteristic size ranging from 2–60 μm) that was swept in the y-direction having a characteristic spacing of 0.5–3 μm. This mesh was predetermined to such that the simulation solution was independent of the mesh density, where typical simulations consisted of 400 000 elements with 1.6 million degrees of freedom. The solution to the velocity, pressure, and concentration fields were obtained using the Generalized Minimal Residual iterative solver, using the successive over-relaxation method for the pre- and post-smoother, and a PARDISO course solver. After convergence of the solutions, the diffusive flux of analyte to the entire sensor surface was calculated as $J = D\ \mathrm{d}C_A/\mathrm{d}y$. The numerical values of J in this study are reported as the average diffusive flux to the 1.9 mm × 0.5 mm interrogation zone shown in Fig. 1.

Experimental methods

SPR sensor. Here we used a 4-channel SPR sensor with wavelength interrogation developed at the Institute of Photonics and Electronics in Prague, Czech Republic.[25] The SPR sensor is based on the Kretschmann configuration of the prism coupler.[26] The sensor consists of an optical module with light source; collimating, polarization and coupling optics; a thermal stabilization module; a spectral analyzing module (4-channel spectrograph); and a sensor head with microfluidic sample delivery to four individual flow chambers. Before introduction into the SPR coupling prism, the polychromatic light is polarized by a thin broad-band polarizer, collimated, and passed through apertures of dimensions 0.5 mm × 1 mm. The beams to individual flow cells are projected to the sensing surface to an area of dimension 0.5 mm × 1.9 mm, referred to herein as the interrogation zone. The incident light is totally reflected at the gold film, which is sufficiently thin to allow penetration of the evanescent field of the incident optical wave through the gold layer. The evanescent field of a particular wavelength can couple with the surface plasmon (SP) propagating at the metal–dielectric interface, where the dielectric in this case is the aqueous solution filling the flow cell. The reflected light from each flow chamber is then

collected into separate optical fibers and coupled to a four-channel spectrograph. Successful optical coupling is manifested as an intensity drop in the wavelength spectrum of reflectivity. Changes in the refractive index near the surface of the gold film (*i.e.* the capture of an analyte *via* a biomolecule) will result in a change in the excitation wavelength of the SPs, measured as a resonance dip in the collected light spectrum. The sensor response is therefore represented by the change in this resonant wavelength and can be calibrated to the change in the surface concentration of bound molecules, where the calibration coefficient is proportional to their molar weight and is dependent on the resonant wavelength. The SPR sensors used in this study have a resonant wavelength of approximately 750 nm, and a 1 nm shift in the resonant wavelength represents a change in the protein surface coverage of 18 ng cm^{-2}.

The flow cells are created using the thick film SU-88 photoresist (Gersteltec Sarl) of varying thickness serving as the channel sidewalls, fabricated onto a CR-39 plastic substrate (Edmund Optics) through which 600 μm holes were drilled to serve as fluidic inputs and outputs. This top layer is then sealed to the sensor floor (SPR chip), consisting of a glass slide (thickness 1.5 mm) having a 50 nm gold film on top of a 2 nm titanium adhesion layer on one side. The SPR chip is optically matched to the SPR coupling prism with the gold-film on top (Fig. 1A). The SU-8 gaskets were created using standard UV lithography, where the height of each gasket was measured using an optical profilometer (Zygo NewView 7300). Each gasket was found to have a surface roughness of less than $0.01 \cdot H$ in the range of $7 < H < 49$ μm. The SU-8/CR39 top layers were sealed to the sensor floor *via* mechanical pressure, where no leaking was observed for the experiments discussed in this study. A peristaltic pump with calibrated volumetric flow rate was used to deliver liquid samples to the flow cell, which was maintained at a constant temperature with a precision of better than 0.01 °C.

Functionalization and detection. The SPR chip was first functionalized with a self-assembled monolayer (SAM) of ω-carboxyalkylthiols on which streptavidin was attached *via* the amide bond. Subsequently, biotinylated oligonucleotides were attached to the streptavidin *via* the streptavidin–biotin interaction. The immobilization procedure is described below. To form a mixed self-assembled monolayer of carboxyl-terminated alkanethiols, the substrates were immersed overnight in 200 μM solution of $HS(CH_2)_{11}(EG)_4OH$ and $HS(CH_2)_{11}(EG)_6OCH_2COOH$ (Prochimia, Poland) in a 7 : 3 ratio. The SPR chip was subsequently rinsed with ethanol and water and further dried with a stream of nitrogen before being mounted into the SPR sensor. Within the flow cell, the carboxylic terminal groups of the alkanethiols were activated with a mixture of 0.5 M 1-ethyl-3-(3-dimethylaminopropyl)-carbodiimide (EDC) and 0.1 M *N*-hydroxysuccinimide (NHS) from GE Healthcare, USA. Subsequently, a 50 μg mL^{-1} solution of streptavidin (Sigma–Aldrich, USA) in 10 mM sodium acetate buffer (pH 5.0) was introduced to the flow-cell for 10 min. Any remaining non-covalently bound streptavidin was then removed with a high ionic strength buffer saline solution. A 100 nM solution of biotinylated DNA probe (Biotin-$(TEG)_2$-5′-GGAAGGGAGTAAAGTTAATA-3′) in tris buffer (pH 7.4) was then pumped over the sensor surface for 10 min. After that time the typical surface concentration of the probes was 4×10^{-14} mol mm^{-2}. For the direct detection of the ssDNA target, we utilized 0.2–100 nM solutions of (5′-TATTAACTTTACTCCCTTCC-3′) in tris buffer with 30 mM $MgCl_2$. Each solution of target ssDNA was injected into the sensing chamber for a period of 10 min, where each concentration was measured at least 3 times on 3 different SPR chips. After this detection step, a buffer was introduced into the sensing chamber for ten minutes, and the bound target was removed with a 2-minute injection of 4 mM glycin (pH 2). The surface densities of both the immobilized probes and the subsequently attached molecules can be calculated using the calibration procedure described in Homola *et al.*[27] For each test, two of the four sensing chambers are utilized for analyte detection under similar conditions, where the remaining two chambers are used as a reference.

Results and discussion

Fig. 2A shows an illustration of the detection method used in the experimental design of this study. Here, we utilize biotinylated 20-mer ssDNA oligomers as capture probes that have been immobilized *via* the biotin–streptavidin interaction

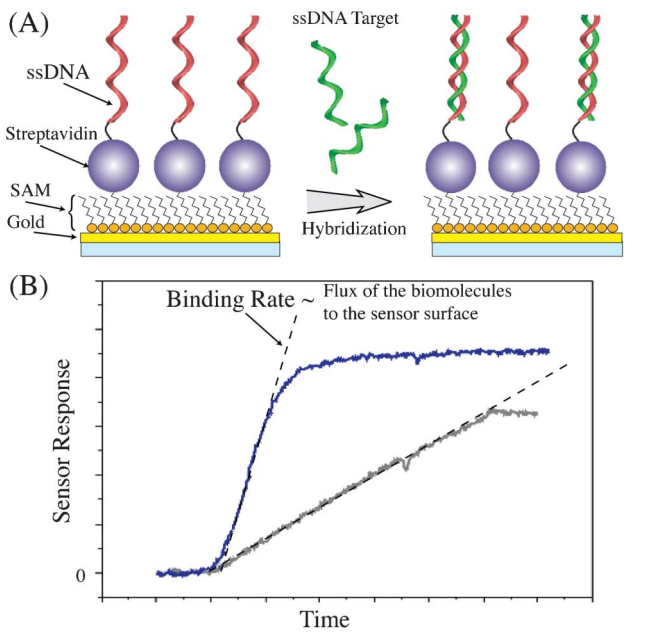

Fig. 2 (A) Scheme of a model biomolecular interaction used in this study. Biotinylated ssDNA is immobilized to a streptavidin layer that is bound to a self-assembled monolayer (SAM) of alkanethiols present on the sensor surface. (B) The typical sensor response *vs.* time, where the blue and grey data sets were taken with higher and lower concentrations of target ssDNA, respectively. The slope of the time-series response is proportional to the flux of analyte to the sensor surface.

to the sensor surface functionalized with SAM of alkanethiols and streptavidin. The surface concentration of probes was $(4 \pm 1) \times 10^{-14}$ mol mm^{-2}. Fig. 2B shows a typical real-time sensor response to the hybridization between the ssDNA probes on the sensor surface and the target molecules for target solution of two different concentrations. When the target ssDNA is introduced into the sensing chamber, the referenced sensor signal will be proportional to the overall mass of captured DNA (*via* hybridization events) in the interrogation region of the sensor (Fig. 1B). More importantly, as seen in Fig. 2B, the rate of the signal increase at the onset of hybridization will be proportional to the flux of ssDNA to the sensor surface, or for the SPR sensor used here, the interrogation region in the center of the sensor chamber. The experimentally determined values of kinetics parameters of the affinity system utilized in this study is $k_1 = 10^7\ M^{-1}\ s^{-1}$, $k_2 = 6 \times 10^{-5}\ s^{-1}$. The ramifications of using a different affinity system will be discussed later.

It is important to know if the design and operation of the SPR-based affinity biosensor shown in Fig. 1 will display a behavior different from the $J \approx H^{-\frac{2}{3}}$ scaling law predicted by eqn (7). Before experimental verification of this scaling law, we first investigate the response of the sensor to changes in H using numerical simulations. The scaling predictions seen in eqn (7) take account of both $L/H \gg 1$ and $W/H \gg 1$, where we assume that the average fluid velocity will be constant over the entire length of the sensor and exist as one dimensional in the z-direction. As seen from Fig. 1B, there is the potential that this assumption is not valid, as the positions of the inlet and outlet in the sensing chamber will lead to both x- and z-components of the velocity having potential effects on the sensor response. To investigate the dependence of the sensing chamber geometry on J, we have utilized the finite element package COMSOL to solve for the analyte flux to the sensor floor under a steady-state assumption. Fig. 3A displays a contour plot of the steady-state diffusive flux of analyte to the sensing chamber floor regarding a sensor with $H = 5$ μm and $Q = 30$ μL min^{-1}. It can be seen that the diffusive flux is highest in the regions directly near the chamber inlet. This is due to both (*a*) the higher fluid velocity in the vicinity of the inlet due to the smaller cross-sectional flow area, and (*b*) the effective length of the sensor in this region being very small, where it follows that δ is small in this region with respect to the rest of the chamber floor. From these results, the analyte flux to the sensor surface is calculated as the average diffusive flux over the interrogation region seen in Fig. 3A. Fig. 3B displays the average steady-state flux to the interrogation region as a function of the chamber height for several volumetric flow rates. It can be seen that the flux increases as the height of the sensor changes, and furthermore, the analyte flux increases with the volumetric flow through the chamber. The data in Fig. 3 pertaining to $H > 20$ μm were then fit to a $J \approx H^{-\frac{2}{3}}$ scaling relationship. It can be seen that the J *vs.* H data fit the $H^{-\frac{2}{3}}$ scaling very well in the range of $H > 20$ μm, whereas the values of $H < 15$ μm lie below the values predicted by that scaling law. It should be noted that the overall difference between the numerical J values from the scaling law prediction decreases as Q increases; for example, the numerical values for $H = 7$ μm are 64%, 85%, and 92% of the predicted result for volumetric flow rates of 10, 20, and 30 μL min^{-1}, respectively.

The results in Fig. 3 show that, for a sensor operating under the parameters in Table 1 (for $H > 20$ μm), numerical simulations predict that the SPR-based biosensor will follow the scaling relationship seen in eqn (7). Following this prediction, we investigated the response of an experimental SPR sensor under the same conditions as those used in Fig. 3B. Fig. 4A details the real-time SPR sensor response for several sensors with varying H concerning the direct detection of 200 pM 20-mer ssDNA at a flow rate of 20 μL min^{-1}. It can be seen that there is a clear increase in the time-derivative of the sensor response as the height of the chamber is reduced. Using the known area of the sensor interrogation zone as well as the relationship between the sensor response and the mass

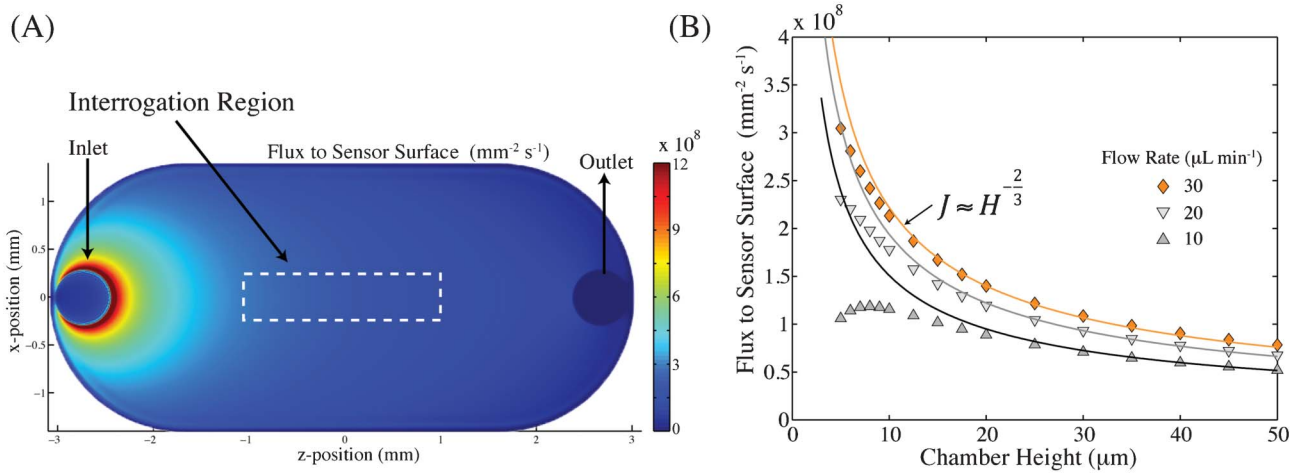

Fig. 3 (A) COMSOL results regarding the flux of an analyte (J) to the sensor chamber floor for a sensor with $H = 5$ μm, $Q = 30$ μL min^{-1}, and $C_{A,o} = 20$ nM. The interrogation region is shown as the white box and is positioned in the center of the chamber. (B) The analyte flux averaged over the interrogation region as a function of the chamber height H. The data points for $H > 15$ μm were fit to the equation $\boldsymbol{J = aH^{-\frac{2}{3}}}$, plotted as the solid lines.

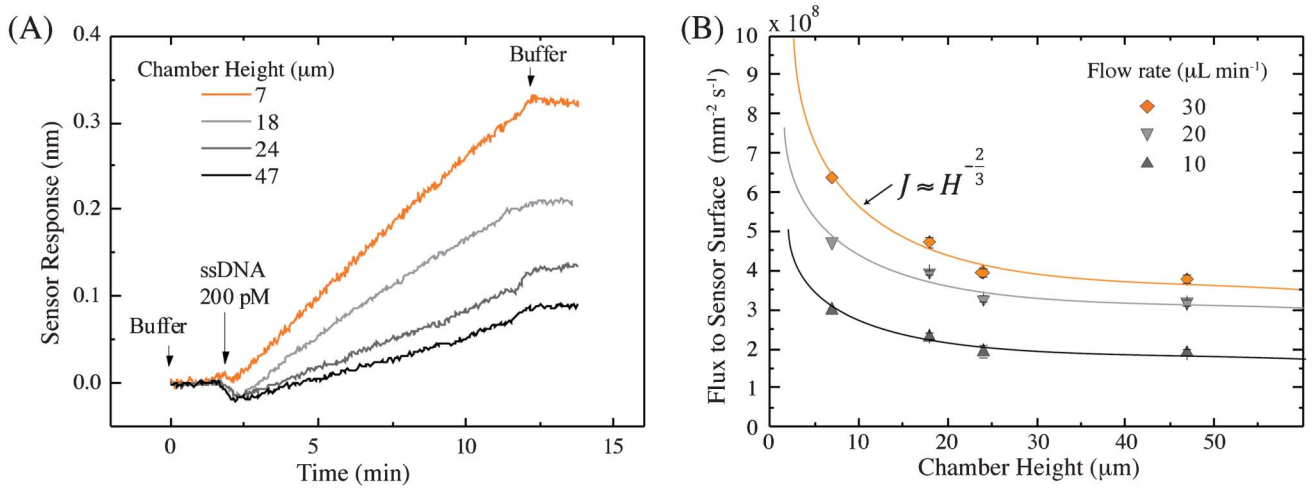

Fig. 4 (A) Sensor response *vs.* time for the direct detection of 200 pM ssDNA. (B) Calculated ssDNA flux to the sensor as a function of chamber height ($C_{A,o}$ = 20 nM). The solid lines represent a fit of the data to a $H^{-\frac{2}{3}}$ scaling law.

of analyte present on the sensing surface, we calculated the flux of analyte towards the sensor surface. These results are highlighted in Fig. 4B, which shows the measured flux of analyte to the sensor surface as a function of chamber height for several volumetric flow rates. These experimental results mirror the results predicted *via* the numerical methods shown in Fig. 3B, as the analyte flux increases for decreasing H and increasing Q. Moreover, as in the case of Fig. 3B, the data in Fig. 4B also follow the $H^{-\frac{2}{3}}$ scaling law, following the trend for the complete range of chamber heights in this study.

The numerical and experimental results seen in Fig. 3 and 4 agree well with respect to their absolute values, where the values of J measured by experiment are higher than those predicted numerically by a factor of approximately 3. An important difference between the two data sets is how they follow the scaling relationship predicted by eqn (7): the experimental data follows $J \approx H^{-\frac{2}{3}}$ for the entire data set, while the numerical data follows this trend only for the range of $H > 20$ μm. It is important to know the parameters that contribute to the small differences observed between these two methods. Next we discuss potential factors that may lead to these differences, and more importantly, how these factors will affect the responses of affinity biosensors of the same principal design.

Given the large number of parameters associated with this study, the small differences in the magnitude of analyte flux between the numerical and experimental results represents a significant accomplishment. These small differences can be attributed to variances in the actual values of the experimental parameters seen in Table 1; however, a likely explanation lies in the differences between how data is collected from both the experimental sensor and the numerical simulation. The sensing head for the experimental SPR sensor used in this study is situated on an adjustable stage, where the x- and z-position of the stage with respect to the incident light beam is tuned to provide optimal sensor performance. Despite the adjustable capability of this sensor, the absolute position of the interrogation region within the boundaries of the sensor chamber floor is not precisely known. From the diffusive flux contours shown in Fig. 3A, it can be seen that the analyte flux will be a function of the (x,z) position of the interrogation zone, where the predicted values of J range from 5.9×10^8 mm^{-2} s^{-1} to 1.4×10^8 mm^{-2} s^{-1} for z-positions of -2 mm and 2 mm, respectively (x = 0). The SPR sensor used herein provides information on C_{AB} only in the regions of the interrogation region, where the response of the sensor will be similar to that of a sensor with a modified length L', where L' is measured from the center of the chamber inlet to the maximum z-value of the interrogation region. Therefore, it is possible that the z-position of the interrogation region for the experimental sensor was situated closer to the chamber inlet with respect to the numerical results (where the interrogation region is in the center of the chamber). From eqn (7), this will be manifested as a higher magnitude of flux with respect to the numerical results (where the interrogation region was centered in the chamber), and helps explain the differences in magnitude between the two plots shown in Fig. 3B and 4B.

Next, we examine the deviation of the scaling behavior at low values of H seen in the numerical results shown in Fig. 3. From these results, it is apparent that this type of sensor will scale as $J \approx H^{-\frac{2}{3}}$ until H falls below a critical height, after which the sensor no longer follows eqn (7). To find out the limitations of this scaling law, we examine the regime in which all of the analyte has the opportunity to interact with capture probes on the sensor surface. The Péclet number can be thought of as the ratio of the characteristic times for diffusion *vs.* convection. By choosing $L/U = HWL/Q$ as the characteristic time for convection (the analyte residence time), we can obtain another form of the Péclet number:

$$\mathrm{Pe_L} = \frac{H^2/D}{HWL/Q} = \frac{1}{\eta}\mathrm{Pe} \tag{8}$$

Therefore a value of $Pe_L \approx 1$ implies that the time for an analyte to diffuse across the entire height of the channel will be equal to the time for the analyte to be transported over the sensor *via* convection. In this regime all of the analyte in the chamber will have the opportunity to interact with the sensor surface, and the system will approach the limit of full collection ($Pe_L < 1$). Here the analyte flux can be calculated as $J = QC_{A,o}/WL$, and J will become independent of the channel height. Using a value of $L'_{num} = 3.5$ mm, we can calculate Pe_L for the three data points concerning $H = 7$ μm in the numerical data shown in Fig. 3B as 0.85, 1.7, and 2.6 for volumetric flow rates of $Q = 10$, 20, and 30 μL min^{-1}, respectively. In this limit of low Pe_L, the sensor is expected to deviate from the scaling behavior observed at higher values of H. In contrast, for $H = 40$ μm, the same values of Pe_L are 6.8, 13.6, and 20.4, and the system is expected to follow the $J \approx H^{-\frac{2}{3}}$ scaling law. This limit of full collection explains the behavior of the $Q = 10$ μL min^{-1} data shown in Fig. 3B, where J starts to decrease in the range of $H < 7$ μm. This behavior can be attributed to the fact that the interrogation region is situated beyond the channel inlet, where the bulk of the analyte capture has taken place in the region of the sensor chamber closer to the chamber inlet. Under the assumption that the difference in the magnitude of Fig. 3B and 4B can be attributed to $L'_{exp} < L'_{num}$, it follows that the critical height for the experimental sensor in this study to approach $Pe_L \approx 1$ is lower than the range tested herein. Hence, it is expected that the results for Fig. 4B will keep to the $J \approx H^{-\frac{2}{3}}$ scaling law.

Fig. 3 and 4 show that (at restricted volumetric flow rates and constant analyte concentrations) significant increases in sensitivity can be obtained *via* decreasing the height of the sensing chamber. It is important to examine how the increase in sensitivity will affect the LOD of the sensor. For assays limited to finite detection times (assuming surface concentration of analyte is less than the equilibrium coverage), an increase in J will result in a higher surface concentration of analyte present on the sensor surface. It follows that an increase in J will also result in a decrease in the "time-to-result," that is, the minimum time required to obtain information regarding the presence (or lack of) an analyte in solution. Furthermore, we expect that for assays restricted to a constant volumetric flow rate, a decrease in H will lead to a decrease in the sensor LOD, as the sensor LOD should be inversely proportional to J. Fig. 5 displays the binding rate of the SPR sensor (proportional to J) as a function of the target analyte concentration for the detection of 20-mer ssDNA. The LOD was determined as a concentration of target equal to three standard deviations of the baseline noise (1×10^{-3} nm min^{-1}). As expected, there is an increase in binding rate as the height of the chamber decreases, where the binding rate increased proportionally across all of the analyte concentrations. This leads to a reduction in the LOD of the sensor by a factor of 4, from 20 pM to 5 pM for the $H = 47$ μm and 7 μm sensing chambers, respectively. These results agree well with eqn (7), where it is predicted that the same decrease in H will result in an increase in flux of $J_{new}/J_{old} \approx (47/7)^{\frac{2}{3}} = 3.5$.

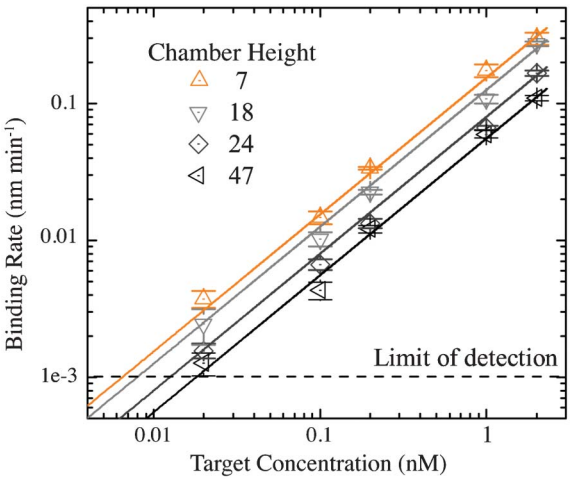

Fig. 5 The maximum binding rate *vs.* concentration for the detection of ssDNA involving the use of chambers with varying H ($Q = 20$ μL min^{-1}). The LOD for each sensor decreases with decreasing H. Each concentration was measured on a minimum of three different SPR chips.

Finally, we address when the scaling relationship seen in eqn (7) will be valid for an affinity-based biosensor. As previously noted, this study involves convective based biosensors operating in the regime of $\eta \gg 1$ and $Pe \gg 1$, where we have invoked a steady-state assumption for mass-transfer limited systems having $Da \gg 1$. Here we address the limitations regarding this steady-state assumption and potential deviations of the behavior of a sensor (operating in the aforementioned regime) from the scaling law seen in eqn (7). Following the results from Squires and Manalis,[20] this assumption is valid when the characteristic time for the depletion layer to form ($\tau_d \approx \delta^2/D$) is much smaller than the characteristic time for the sensor to reach an equilibrium state (τ_{CRD}). This can be expressed in equation form as

$$\varepsilon = \frac{\tau_d}{\tau_{CRD}} \approx 0.3 \frac{k_2}{k_1} \frac{L}{C_{B,o}} \eta^{-\frac{4}{3}} Pe^{-\frac{1}{3}} \ll 1 \quad (9)$$

where we are considering the use of such a device towards the detection of analyte present in low concentrations ($C_{A,o} \ll k_2/k_1$), and the analyte boundary layer is not fully developed ($\delta < H$, or $L < 0.1 \cdot HPe$). For situations where the boundary layer is fully developed,[28] eqn (9) will reduce to

$$\varepsilon \approx 2.4 \frac{k_2}{k_1} \frac{L}{C_{B,o}} \eta^{-1} \ll 1 \quad (10)$$

So far this study has assumed that $\varepsilon \ll 1$, where steady-state simulations of the sensor are in good agreement with experimental results. Obviously, an experimental system can be designed such that $Pe \gg 1$ and $\varepsilon \geqslant 1$ (such as a sensor with a very low concentration of surface probes). In this case, δ will no longer be independent of time and eqn (6) will no longer remain valid. However, there are very few biosensing devices that fall under this category (for $\eta \gg 1$ and $Pe \gg 1$), and the

details of the sensor response in this regime are outside the scope of this study.

As discussed above, the scaling law seen in eqn (7) will remain valid for affinity-based biosensors falling under the regime of Pe $\gg$ 1, Da $\gg$ 1, and Pe $>$ η. For these systems, a reduction in the dimensions of the flow cell under a constant volumetric flow rate will provide increases in sensitivity, scaling as both $J \approx H^{-\frac{2}{3}}$ and $J \approx W^{-\frac{1}{3}}$, as long as the system can tolerate the smaller dimensions (*e.g.* no fluid leaking as a result of an increased fluidic resistance from decreases in H). It is important to note that these results will remain valid independent of the transduction method of the biosensor; the result of this study will benefit sensors using mechanical, optical, electrical, and any other detection methods using an affinity-based biocomponent. These results are also applicable to other microfluidic systems using a planar surface as an active component, including microreactors based on surface catalyzed reactions as well as micro-fuel cells; however, the parallels between these systems and affinity-based biosensors is beyond the scope of this study.

Conclusions

Here we have presented a generalized method to improve the sensitivity of microfluidic affinity-based biosensors operating with constant volumetric flow rates such that the mass transfer Péclet number (Pe = Q/WD) is larger than the channel aspect ratio ($\eta = L/H$), or simply Pe $>$ η. Starting with the assumption that a sensor is in the regime of Pe $\gg$ 1 with a Damköhler number of Da $\gg$ 1, we have derived a scaling law that predicts the analyte flux to the sensor to scale as $J \approx H^{-\frac{2}{3}}$ for systems with constant volumetric flow rate, and $J \approx H^{-\frac{1}{3}}$ for systems with constant average fluid velocity. This scaling behavior has been verified using both (*a*) the finite element solver COMSOL and (*b*) an experimental SPR-based biosensor involving the detection of 20-mer oligomers of ssDNA. Both the numerical and experimental results were found to follow the scaling law in the range of Pe $>$ η. For biosensors operating in this regime, the increase in analyte flux by a reduction in H will result in a significant decrease in the LOD. We demonstrate this enhancement by demonstrating the effect of a reduction of H on the LOD of an SPR-based biosensor, where we show an improvement in the LOD from 20 pM to 5 pM by reducing the sensing chamber height from 47 μm to 7 μm.

Acknowledgements

This research was supported by Praemium Academiae of the Academy of Sciences of the Czech Republic and by the Czech Science Foundation under contract # P205/12/G118.

References

1 R. J. O'kennedy, P. J. Conroy, S. Hearty and P. Leonard, *Semin. Cell Dev. Biol.*, 2009, **20**, 10–26.
2 K. Sefah, J. A. Phillips, X. L. Xiong, L. Meng, D. Van Simaeys, H. Chen, J. Martin and W. H. Tan, *Analyst*, 2009, **134**, 1765–1775.
3 C. Gronwall and S. Stahl, *J. Biotechnol.*, 2009, **140**, 254–269.
4 X. D. Fan and I. M. White, *Nat. Photonics*, 2011, **5**, 591–597.
5 J. L. Arlett, E. B. Myers and M. L. Roukes, *Nat. Nanotechnol.*, 2011, **6**, 203–215.
6 J. S. Daniels and N. Pourmand, *Electroanalysis*, 2007, **19**, 1239–1257.
7 J. Homola, H. Vaisocherová, J. Dostálek and M. Piliarik, *Methods*, 2005, **37**, 26–36.
8 S. Prakash, M. Pinti and B. Bhushan, *Philos. Trans. R. Soc. London, Ser. A*, 2012, **370**, 2269–2303.
9 J. D. Kirtland, G. J. McGraw and A. D. Stroock, *Phys. Fluids*, 2006, **18.**
10 J. D. Kirtland, C. R. Siegel and A. D. Stroock, *New J. Phys.*, 2009, **11.**
11 R. A. Vijayendran, F. S. Ligler and D. E. Leckband, *Anal. Chem.*, 1999, **71**, 5405–5412.
12 V. Sikavitsas, J. M. Nitsche and T. J. Mountziaris, *Biotechnol. Prog.*, 2002, **18**, 885–897.
13 K. Sigmundsson, G. Masson, R. H. Rice, N. Beauchemin and B. Obrink, *Biochemistry*, 2002, **41**, 8263–8276.
14 D. G. Myszka, X. He, M. Dembo, T. A. Morton and B. Goldstein, *Biophys. J.*, 1998, **75**, 583–594.
15 D. Erickson, *Microfluid. Nanofluid.*, 2005, **1**, 301–318.
16 W. Zhang, H. A. Stone and J. D. Sherwood, *J. Phys. Chem.*, 1996, **100**, 9462–9464.
17 T. Gervais and K. F. Jensen, *Chem. Eng. Sci.*, 2006, **61**, 1102–1121.
18 R. Hansen, H. Bruus, T. H. Callisen and O. Hassager, *Langmuir*, 2012, **28**, 7557–7563.
19 T. M. Squires and S. R. Quake, *Rev. Mod. Phys.*, 2005, **77**, 977–1026.
20 T. M. Squires, R. J. Messinger and S. R. Manalis, *Nat. Biotechnol.*, 2008, **26**, 417–426.
21 H. Šípová, S. L. Zhang, A. M. Dudley, D. Galas, K. Wang and J. Homola, *Anal. Chem.*, 2010, **82**, 10110–10115.
22 H. Šípová, V. Ševců, M. Kuchař, J. N. Ahmad, P. Mikulecký, P. Šebo, P. Malý and J. Homola, *Procedia Engineer*, 2011, **25.**
23 M. Vala, S. Etheridge, J. A. Roach and J. Homola, *Sens. Actuators, B*, 2009, **139**, 59–63.
24 R. B. Bird, W. E. Stewart and E. N. Lightfoot, *Transport phenomena*, J. Wiley, New York, 2002.
25 H. Vaisocherová, K. Mrkvová, M. Piliarik, P. Jinoch, M. Steinbachová and J. Homola, *Biosens. Bioelectron.*, 2007, **22**, 1020–1026.
26 H. Raether, *Springer Tracts Mod. Phys.*, 1988, **111**, 1–133.
27 J. R. Homola, *Surface plasmon resonance based sensors*, Springer, Berlin, New York, 2006.
28 For the geometry considered in this study the dimensionless analyte flux towards the sensing surface (known as the Sherwood number) will converge to a value of approximately 2.4 for a fully developed boundary layer.